ELSEVIER

www.elsevier.nl/locate/jorganchem

Journal of Organometallic Chemistry 614–615 (2000) 92–98

Journal of Organometallic Chemistry

# Comparison of the geometric and molecular orbital structures of $(Cp^*Cr)_2B_4H_8$ and $(Cp^*Re)_2B_4H_8$, $Cp^* = \eta^5$-$C_5Me_5$. Structural consequences of delocalized electronic unsaturation in a metallaborane cluster

Sundargopal Ghosh, Maoyu Shang, Thomas P. Fehlner *

*Department of Chemistry and Biochemistry, University of Notre Dame, 261 Nieuwland Science, Notre Dame, IN 46556-5670, USA*

Received 6 March 2000; accepted 25 May 2000

Dedicated to Professor Sheldon G. Shore on the occasion of his 70th birthday.

**Abstract**

Comparison of the structures of two metallaboranes possessing the same borane fragment and ancillary metal ligands but differing transition metal atoms defines the geometric consequences of the addition (or removal) of two valence electrons from a bicapped tetrahedral metallaborane cluster structure. Likewise the effects of the cluster distortion on electronic structure is explored utilizing approximate molecular orbital calculations on hypothetical $(CpMn)_2B_4H_8$, $Cp = \eta^5$-$C_5H_5$, as it is changed from the shape characteristic of five skeletal electron pair (sep) $(Cp^*Cr)_2B_4H_8$ to that of six sep $(Cp^*Re)_2B_4H_8$, $Cp = \eta^5$-$C_5Me_5$. In doing so it is demonstrated that the observed changes in the metal–metal distance (a counter-intuitive increase with smaller sep) and endohydrogen positions (more like B–H with smaller sep) are required to electronically accommodate the removal of a pair of electrons from a saturated bicapped tetrahedral cluster. 

*Keywords:* Cluster; Metallaborane; Chromium; Rhenium; Boron; MO

## 1. Introduction

The isolation and characterization of the chromaborane $(Cp^*Cr)_2B_4H_8$ (**1**), $Cp^* = C_5Me_5$, created an interesting problem in that its skeletal electron count [1,2] is two electrons less than required for the bicapped tetrahedral geometry displayed [3,4]. Clusters displaying this property are considered to be electronically unsaturated [5]. Some unsaturated clusters display a localized M–M multiple bond [6], whereas the geometric structure of **1** suggests unsaturation delocalized throughout the cluster bonding network. The observed structural response of the $Cr_2B_4$ skeleton to the addition of CO, $CS_2$, and $Fe(CO)_3$ moieties when analyzed by molecular orbital (MO) methods supports this interpretation [7]. Subsequent comparison with the behavior of molybdaboranes adds corroboration [8,9], as does the ready formation of the radical anion $[(Cp^*Cr)_2B_4H_8]^-$ from **1** [10].

### 1.1. Why revisit this problem?

Taken as a whole the evidence for viewing **1** as an example of an unsaturated metallaborane is convincing but each comparison involves at least one reasonable, but unproved, assumption. Even the skeletal electron count presupposes a nonbonding role for a set of metal based electrons. Thus, we continued to seek the definitive comparison — a metallaborane possessing the same ancillary metal ligands and an identical borane fragment, i.e. $(Cp^*M)_2B_4H_8$, M = Group 7 metal (Scheme 1). The only difference between **1** and this compound would be the number of electrons brought to cluster bonding by the metals. Questions of how to partition electrons between dissimilar fragments would be eliminated and the parameters of the formally saturated compound could then be directly compared with those of **1**.

* Corresponding author. Fax: +1-219-6316652.
*E-mail address:* fehlner.1@nd.edu (T.P. Fehlner).

0022-328X/00/$ - see front matter 
PII: S0022-328X(00)00303-X

An Mn derivative would be ideal, but, to date, it has eluded us. There are only a few examples of rhenaboranes [11–14], however, the reaction of $Cp^*ReCl_4$ with $Li[BH_4]$ as per our general method [9] produced a satisfactory alternative, $(Cp^*Re)_2B_4H_8$ (**2**). In the following we present a detailed analysis of the structural parameters and show that the principal differences between $(Cp^*M)_2B_4H_8$, M = Cr and Re, are fully in accord with MO requirements for the stabilization of the additional pair of electrons. A structural mechanism, both geometric and electronic, whereby **1** adjusts to the absence of a pair of cluster bonding electrons is defined.

## 2. Experimental

### 2.1. General experimental information

All the operations were conducted under Ar atmosphere using standard Schlenk technique. Solvents were distilled prior to use under $N_2$. $BH_3$·THF (1.0 M in THF), $LiBH_4$ (2.0 M in THF), $PPh_3$, $SiMe_3Cl$ (Aldrich) and $Cp^*Re(CO)_3$ (Strem) were used as received without standardization. $O_3$ gas was generated from an ozone generator (OSMONICS, OREC™ Ozone Generator; V series), operating at 0.9 amp.

NMR spectra were recorded on a 300 or 500 MHz Varian FT-NMR spectrometer. Residual solvent protons were used as reference ($\delta$, ppm, benzene, 7.15), while a sealed tube containing $[Me_4N(B_3H_8)]$ in acetone-$d_6$ ($\delta_B$, ppm, −29.7) was used as an external reference for the $^{11}$B-NMR. Infrared spectra were obtained on a Nicolet 205 FTIR spectrometer. Mass spectra were obtained on JOEL JMS-AX505HA mass spectrometer with perfluoro kerosene as standard. $Cp^*ReCl_4$ is prepared by the treatment of the oxo–rhenium complex, $Cp^*ReO_3$ [15] with chlorotrimethylsilane in the presence of the Lewis base, triphenylphosphine [16].

### 2.2. Synthesis of $(Cp^*ReH_2)_2B_4H_4$ (2)

In a typical reaction, $Cp^*ReCl_4$ (0.25 g, 0.54 mmol) was dissolved in 15 ml of freshly distilled toluene to generate a purple solution. The mixture was chilled to −40°C and five equivalents of $LiBH_4$ (1.3 ml, 2.69 mmol) were added slowly. The reaction mixture was allowed to warm slowly to room temperature (r.t.) and within 5 min the purple suspension had turned greenish–yellow, accompanied by the evolution of $H_2$. After stirring for 1 h at r.t., the solvent was removed under vacuum. Extraction with hexane gave a yellow solution that was heated at 65°C for 1 h. The solvent was again removed, the residue extracted in hexane, filtered through 2 cm of celite and concentrated for crystallization. Most of the $Cp^*ReH_6$ (slightly yellow) and $(Cp^*Re)_2H_6$ (yellowish–brown) come out at −40°C after 3 days. Filtration and concentration of the mother-liquor gave orange–yellow crystals of **2** on crystallization at −40°C over night (yield = 32% based on rhenium). MS (EI), $P^+_{max} = 692$, isotope distribution pattern for 2Re, 4B atoms. Calculated for weighted average of isotopomers lying within the instrument resolution, 694.2305, observed, 694.2282. $^{11}$B-NMR ($C_6D_6$, 22°C, $\delta$): 68.7 (d, $J_{B-H} = 154$ Hz, 2B), 1.3 (d, $J_{B-H} = 166$ Hz, 2B); $^1$H-NMR ($C_6D_6$, 22°C, $\delta$): 9.3 [partially collapsed quartet (pcq), 2BHt], 1.96 (s, 30H, 2Cp*), 0.7 [pcq, 2BH*t*], −11.52 [s, 4H, Re–H]. IR (KBr, $cm^{-1}$): 2506w, 2468w (B–H). $^{13}$C-NMR ($C_6D_6$, 22°C): $\delta$ 97.14 ($C_5(CH_3)_5$); $\delta$ 13.25 ($C_5(CH_3)_5$).

### 2.3. Molecular structure of 2

Orange–yellow, air-sensitive, thread like-crystals of $(Cp^*ReH_2)_2B_4H_4$ (**2**) were grown by slow cooling of a hexane solution at −40°C. The crystal selected was mounted in a capillary under argon prior to data collection. compound **2** crystallizes in tetragonal $P4_2/n$, $a = b = 23.9432$ (15), $c = 8.385$ (2) Å, $V = 4806.8$ (13)

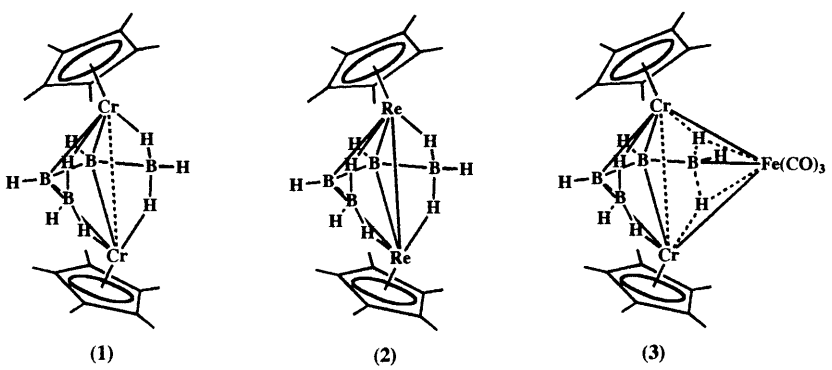


Scheme 1.

Table 1
Crystal data for $Cp^*_2Re_2B_4H_8$ (**2**)

| | |
|---|---|
| Empirical formula | $C_{20}H_{38}B_4Re_2$ |
| Formula weight | 694.14 |
| Crystal system | Tetragonal |
| Space group | $P4_2/n$ |
| Unit cell dimensions | |
| $a$ (Å) | 23.9432(15) |
| $b$ (Å) | 23.9432(15) |
| $c$ (Å) | 8.385(2) |
| Volume (Å$^3$) | 4806.8(13) |
| $Z$ | 8 |
| $D_{calc}$ (mg m$^{-3}$) | 1.918 |
| $F(000)$ | 2624 |
| Wavelength (Å) | 0.71073 |
| Absorption coefficient (mm$^{-1}$) | 10.066 |
| Crystal size (mm) | $0.45 \times 0.10 \times 0.07$ |
| Temperature (K) | 293(2) |
| Diffractometer | Enraf–Nonius CAD4 |
| Theta range for data collection (°) | 2.41–25.00 |
| Index ranges | $0 \le h \le 28$, $0 \le k \le 28$, $0 \le l \le 9$ |
| Scan method | $\omega/2\theta$ |
| Scan rate (° min$^{-1}$ (in $\omega$)) | 1.37–8.24 |
| Scan width (° (in $\omega$)) | $0.70 + 0.35 \tan\theta$ |
| Total data collected | 4440 |
| Unique data | 4221 [$R_{int} = 0.0403$] |
| Unique observed data [$I > 2\sigma(I)$] | 2057 |
| Absorption correction | Psi-scan |
| Max and min transmission | 0.994 and 0.715 |
| Refinement method | Full-matrix on $F^2$ (SHELXL-93) |
| Weighting scheme | sigma weight |
| Data/restraints/parameters | 4221/20/238 |
| Goodness-of-fit on $F^2$ | 0.965 |
| Final $R$ indices [$I > 2\sigma(I)$] | $R_1 = 0.0533$, $wR_2 = 0.1060$ |
| $R$ indices (all data) | $R_1 = 0.1253$, $wR_2 = 0.1268$ |
| Extinction coefficient | 0.00002(2) |
| Largest difference peak and hole (e Å$^{-3}$) | 0.955 and −1.180 |

Å$^3$. Data collection with Mo–$K_\alpha$ radiation ($l = 0.71073$ Å) was carried out on an Enraf–Nonius CAD4. Structure solution and refinement were performed on a PC by using the SHELXTL package [17]. Most of the nonhydrogen atoms were located by the direct method, the remaining nonhydrogen atoms were found in succeeding difference Fourier synthesis. Least-squares refinement was carried out on $F^2$ for all reflections. All reflections, including those with negative intensities, were included in the refinement and the $I > 2\sigma(I)$ criterion was used only for calculating $R_1$. The maximum and minimum residual electron densities on the final difference Fourier map were 0.971 and −1.189 e Å$^3$, respectively. All estimated S.D. values were estimated by the use of the full covariance matrix. The cell estimated S.D. values were included in the estimation of estimated S.D. values of bond distances and angles. The crystal data are given in Table 1 and selected bond distances and bond angles in Table 2.

### 2.4. Calculational method

The molecular orbital calculations were carried out on hypothetical $Cp_2Mn_2B_4H_8$, $Cp = \eta^5$-$C_5H_5$, using the Fenske–Hall approximate MO method [18,19]. The 1988 version for Macintosh computers utilizing a minimal basis set was employed. For simplicity, a Cp ligand on the Mn atom was used in place of the Cp* ligand found in the actual compounds modeled, i.e. $Cp^*_2Cr_2B_4H_8$ (**1**) and $Cp^*_2Re_2B_4H_8$ (**2**) (Scheme 1). Coordinates were taken from the X-ray crystallographic data and idealized where appropriate [3]. Calculations were carried out on $Cp_2Mn_2B_4H_8$ in the structure of **1** as the endo-hydrogen positions in **1** are defined by the structure study whereas those in **2** were not. The cluster was then distorted to mimic the small, but significant, changes observed in going from **1** to **2**. Although the hydrogens associated with the rhenium atoms were not determined in the structure analysis, reasonable positions were generated utilizing structural data from model compounds as well as $^1$H-NMR data (Section 3).

## 3. Results and discussion

The qualitative cluster structures exhibited by $(Cp^*M)_2B_4H_8$, M = Cr (**1**), Re (**2**), are shown in

Table 2
Selected bond distances (Å) and angles (°) for $Cp^*_2Re_2B_4H_8$ (**2**) $Cp^*_2Re_2B_4H_8Fe(CO)_3$ (**3**)

| | | | |
|---|---|---|---|
| *Bond distances* | | | |
| Re(1)–B(3) | 2012(2) | Re(2)–B(4) | 2.11(3) |
| Re(1)–B(4) | 2.16(3) | Re(2)–B(1) | 2.19(3) |
| Re(1)–B(1) | 2.22(3) | Re(2)–B(2) | 2.17(2) |
| Re(1)–B(2) | 2.21(3) | B(1)–B(2) | 1.74(4) |
| Re(1)–Re(2) | 2.8091(8) | B(2)–B(3) | 1.94(5) |
| Re(2)–B(3) | 2.10(3) | B(3)–B(4) | 1.64(4) |
| *Bond angles* | | | |
| B(3)–Re(1)–B(4) | 45.0(12) | B(2)–Re(2)–Re(2) | 50.8(7) |
| B(3)–Re(1)–B(1) | 88.3(13) | B(2)–B(1)–Re(2) | 65.7(15) |
| B(4)–Re(1)–B(1) | 96.6(12) | B(2)–B(1)–Re(1) | 66.6(15) |
| B(3)–Re(1)–B(2) | 53.1(14) | Re(2)–B(1)–Re(1) | 79.0(11) |
| B(4)–Re(1)–B(2) | 88.0(13) | B(1)–B(2)–B(3) | 111(2) |
| B(1)–Re(1)–B(2) | 46.3(12) | B(1)–B(2)–Re(2) | 67.3(12) |
| B(3)–Re(1)–Re(2) | 47.8(7) | B(3)–B(2)–Re(2) | 61.1(12) |
| B(4)–Re(1)–Re(2) | 48.0(9) | B(1)–B(2)–Re(1) | 67.2(12) |
| B(1)–Re(1)–Re(2) | 50.1(8) | B(3)–B(2)–Re(1) | 61.0(13) |
| B(2)–Re(1)–Re(2) | 49.4(6) | Re(2)–B(2)–Re(1) | 79.8(10) |
| B(3)–Re(2)–B(4) | 45.9(13) | B(4)–B(3)–B(2) | 116(2) |
| B(3)–Re(2)–B(1) | 89.7(12) | B(4)–B(3)–Re(2) | 67.4(16) |
| B(4)–Re(2)–B(1) | 99.0(11) | B(2)–B(3)–Re(2) | 64.9(12) |
| B(3)–Re(2)–B(2) | 54.0(14) | B(4)–B(3)–Re(1) | 68.7(16) |
| B(4)–Re(2)–B(2) | 90.5(13) | B(2)–B(3)–Re(1) | 65.9(12) |
| B(1)–Re(2)–B(2) | 47.1(12) | Re(2)–B(3)–Re(1) | 83.6(9) |
| B(3)–Re(2)–Re(1) | 48.5(6) | B(3)–B(4)–Re(2) | 66.7(17) |
| B(4)–Re(2)–Re(1) | 49.6(9) | B(3)–B(4)–Re(1) | 66.2(14) |
| B(1)–Re(2)–Re(1) | 50.9(7) | Re(2)–B(4)–Re(1) | 82.4(12) |

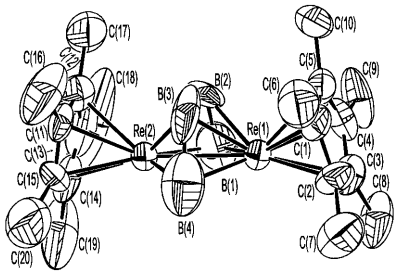


Fig. 1. Molecular structure of $(Cp^*Re)_2B_4H_8$ (**2**).

Scheme 1 and the solid state structure of **2** is given in Fig. 1. The compounds are described as $(Cp^*M)_2(BH)_2$ dimetallatetrahedranes capped on each $M_2B$ face with a $BH_3$ group such that the extra two hydrogens reside on the 'butterfly' shaped face thereby generated. Based on the capping principle [2] the skeletal electron count is determined by the central polyhedron, i.e. the $M_2B_2$ tetrahedron, and is six skeletal electron pairs (sep). Formally, Cp*Re contributes zero sep; hence for M = Re, six sep are available and the observed structure obeys the counting rules. The compound with M = Cr possesses five sep and does not obey the rules for the geometry observed. Further capping, which is observed in larger systems [20], is impossible and, unlike the analogous organometallic system mentioned above, no localized Cr–Cr multiple bonds are formed [6]. As the qualitative cluster shapes of **1** and **2** are the same, differences are sought in the magnitude of the structural parameters and the positioning of the endo–hydrogen atoms.

### 3.1. Differences in geometric structures

The important geometrical differences between the bicapped tetrahedral cores of $(Cp^*M)_2B_4H_8$, M = Cr, Re, are shown in Fig. 2 and Table 3. These parameters are also compared with those of the $Cr_2B_4$ core of $(Cp^*Cr)_2B_4H_8Fe(CO)_3$ (**3**) [21], which we used previously as a model for a six sep saturated cluster [7]. In the older study, the $[(Cp^*Cr)_2B_4H_8]^{2-}$ fragment was assumed to be a complex six electron ligand bound to a $[Fe(CO)_3]^{2+}$ fragment. The principal differences between **1** and **3** are a shorter Cr–Cr distance and longer Cr–B distances both of which can be generated by a compression of the $Cr_2B_4$ core along the Cr–Cr direction on the addition of two electrons.

The existence of compound **2** permits a structural comparison without the perturbations caused by additional metal fragments or different ancillary ligands on the metals. However, as the Mn analog of **1** is not available, comparison with **2** does require a correction for the difference between the covalent radii of Re and Cr of ca. 0.1 Å. Even without this correction, the shortening of the M–M distance on the addition of two electrons is confirmed, i.e. the Cr–Cr distance in **1** is significantly longer than the Re–Re distance in **2**. As discussed elsewhere [4], the Cr–Cr distance in **1** is longer than a 'normal' single bond distance (but not the longest known) whereas the Re–Re distance in **2**, is in the range observed for a bond of order one [22]. On the other hand, the increase in average M–B distance (**1** vs. **3**) is not confirmed. In contrast, the distortion in going from **1** to **2** causes the B–B distance of the central

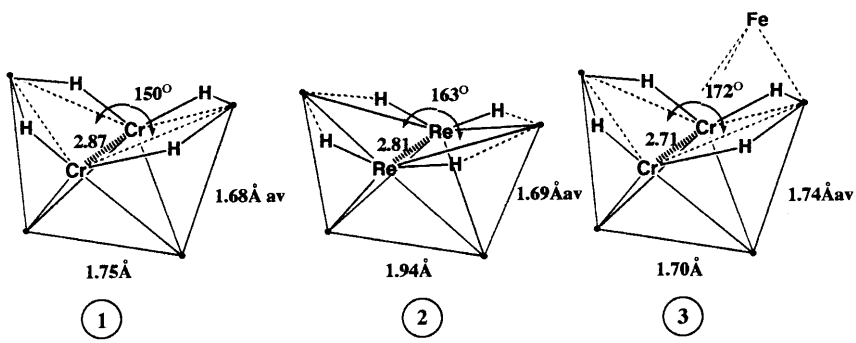


Fig. 2. Geometric, chemical shift and coupling constant differences between the cluster cores of $(Cp^*M)_2B_4H_8$, M = Cr (**1**), Re (**2**) and $(Cp^*Cr)_2B_4H_8Fe(CO)_3$ (**3**). The solid dots represent BH fragments.

Table 3
Selected structural parameters of $Cp^*_2Cr_2B_4H_2$ (**2**), $Cp^*_2Cr_2B_4H_8Fe(CO)_3$ (**3**)

| Compound | sep | d(M–M) (Å) | Average *d*(M–B) (Å) | Average *d*(B–B) (Å) | Average B–B–B (°) |
|---|---|---|---|---|---|
| **1** | 5 | 2.87 | 2.06 | 1.70 | 112 |
| **2** | 6 | 2.81 | 2.17 | 1.77 | 113 |
| **3** | 6[a] | 2.71 | 2.17 | 1.72 | 121 |

[a] Assumed in fragment analysis of the compound as $[Cp^*_2Cr_2B_4H_8]^{2-}$ and $[Fe(CO)_3]^{2+}$.

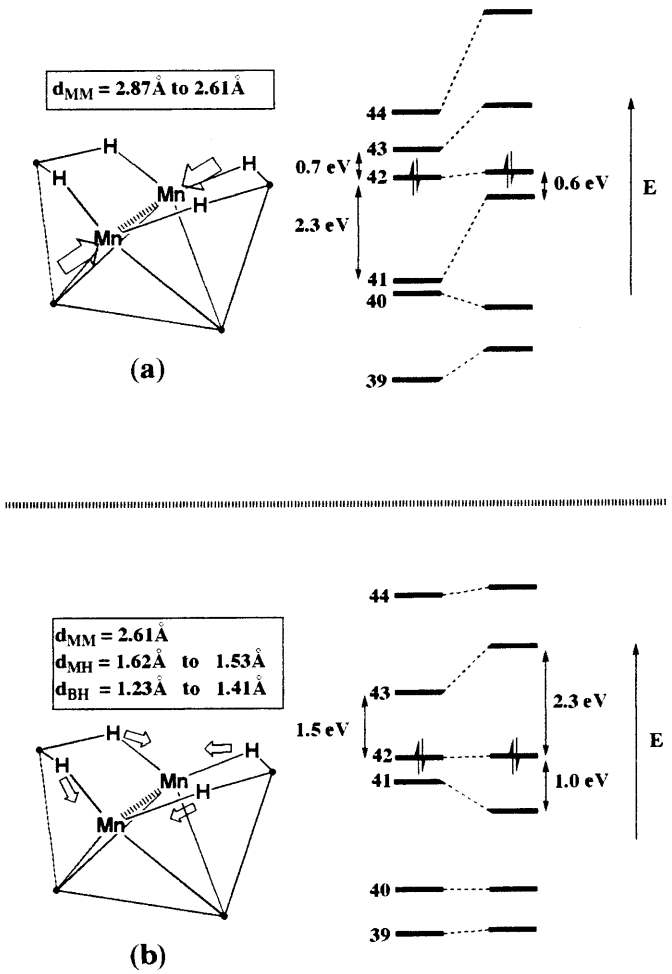


Fig. 3. Correlation diagram showing the change in energy of the frontier MO values of $Cp_2Mn_2B_4H_8$ as the Mn–Mn distance is shortened (a) and the endo hydrogens are moved away from B towards Mn (b) as described in the text.

$Re_2B_2$ tetrahedron to increase while largely retaining the dihedral angle of the hydrogen bridged 'butterfly' face. The increased B–B distance may well reflect the larger metal radius of Re versus Cr more than effects of compressing the core. Thus, the major geometric change is simply shortening of the M–M distance — a change which is counter intuitive in that in a normal cluster addition of a pair of electrons causes bond breakage. On the other hand, in **3** the three B–B distances are nearly equal and the 'butterfly' face is nearly flat — both differences presumably a result of the effects of coordination to the iron fragment.

In the previous analysis the differences between **1** and **3** (and two other derivatives) were adequately explained without consideration of a role for the four endo hydrogen atoms, the characterization of **2** shows that these cannot be neglected. Even though the endo hydrogen atoms were not located in the structure determination of **2**, the $^1$H-NMR resonances of these hydrogens reveal a striking difference between **1** and **2**. The $^1$H chemical shift and coupling constant for the endo hydrogens of **1** are $\delta$ −3.9 and $J_{B-H}$ ca. 70 Hz whereas they are $\delta$ −11.5 and $J_{B-H}$ ca. 15 Hz for **2**. The chemical shift exhibited by **1** is to lower field than typically observed for a M–H–B hydrogen and in the range observed for B–H–B hydrogens. Also, the coupling constant is larger than usually observed and almost as large as found in a $BH_3$ base adduct. Both observations suggest high B character in the B–H bond and a stronger interaction with the boron atom than with the chromium atom. On the other hand, the high field chemical shift exhibited for **2** is in the range typical of a M–H–M or M–H–B bridging hydrogen but the coupling constant observed (selective $^1$H{$^{11}$B} decoupling) suggests a weak interaction with boron. In short, these parameters suggest highly asymmetric M–H–B endo hydrogens with the asymmetry exactly the opposite in the two molecules.

In summary, in going from **1** to **2** the M–M distance decreases and the bridging hydrogens change from mainly boron bonding to mainly metal bonding. The former corroborates the earlier comparison of **1** with **3**; however, no information on the latter was evident previously as the $Fe(CO)_3$ fragment in **3** is bound to one $Cr_2B$ triangle via two endo hydrogens (Scheme 1).

### 3.2. Differences in frontier MO structures

One expects these geometric changes to be reflected in changes in the electronic structures and the latter has been explored using a molecular orbital model. The MO structure of **1**, which has been discussed in detail previously [7,9], provides the starting point. The pertinent MO values, all of which have large metal characters, are illustrated in Fig. 3(a) and Fig. 4 for $Cp_2Mn_2B_4H_8$. MO values 39–44 are derived largely from the 3d Mn orbitals of the Cp*Mn fragments [23]. MO 40 and 44, $d_{z^2}$, are $\sigma$ metal–metal bonding and antibonding, respectively and account for the weak, but real, Cr–Cr bond in **1**. This point was discussed previously [4]. MO 42 and 41, $d_{x^2-y^2}$, are $\delta$ metal–metal bonding and antibonding, respectively, and the latter is the HOMO in **1** whereas, the former is the HOMO in **2**. Finally, MO 43 and 39, $d_{xy}$, are $\delta$ metal–metal bonding and antibonding.

The cluster structure change mimicking **1** to **2** is carried out in two steps. In the first step, the Mn–Mn distance of $Cp_2Mn_2B_4H_8$ is decreased from 2.87 to 2.61 Å (from the M–M distance in **1** to the M–M distance in **2** corrected for the difference in metal radii) and the perturbation in the frontier orbitals is shown in the abbreviated correlation diagram in Fig. 3(a). The MO values respond to the perturbation as follows. The splitting between MO 40 and 44 increases as expected based on their essential association with Mn–Mn $\sigma$ bonding. The MO 43, 39 pair both increase in energy as

both have considerable boron content of M–B antibonding character which is increased by moving the metal atoms together. MO 41 rises in energy and becomes nearly degenerate with the MO 42. The change is not due to the metal–metal $\delta$ antibonding character as its bonding partner, MO 42, varies little in energy. Rather, with the endo hydrogens positioned as in **1**, the Mn–H interaction is largely antibonding and becomes larger as the metals are moved together.

These changes have consequences. As MO 41 is the HOMO of **1** a short M–M distance destabilizes the cluster structure for chromium. On the other hand, the HOMO of **2** is MO 42 and the increased energy gap between MO values 42 and 43 caused by the shorter Mn–Mn distance suggests better stability for this electron count. The same qualitative changes in the MO energies were observed when **1** was distorted into the structure observed in **3** [7]. That is, the structural change provided an ideal orbital situation for binding **1** to the $Fe(CO)_3$ fragment generating the suggestion that the iron fragment effectively contributes two electrons to the $Cp^*_2Cr_2B_4H_8$ 'ligand'.

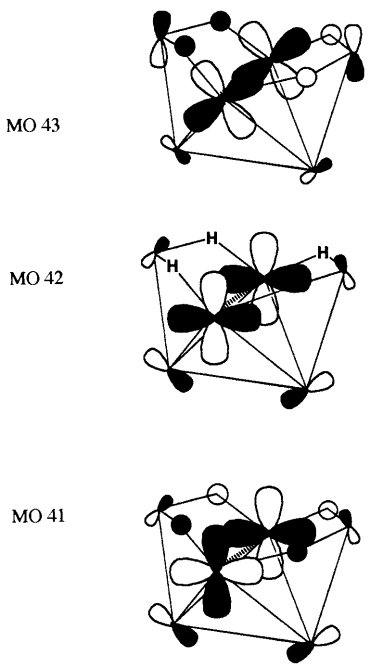


Fig. 4. Schematic drawings of the atomic orbital contributions to the frontier orbitals of $Cp_2Mn_2B_4H_8$.

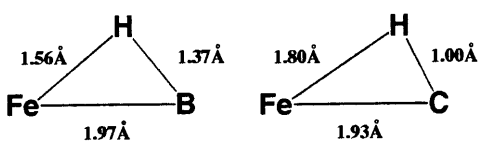


Fig. 5. Difference in placement of the bridging hydrogen atom in $HFe_4(CO)_{12}BH_2$ and $HFe_4(CO)_{12}CH$.

In the second step the placement of the endo hydrogens are adjusted to mimic the change from **1** to **2**. The starting point for the calculations is $Cp_2Mn_2B_4H_8$ with the geometry of **1** but with an Mn–Mn distance of 2.61 Å. To model the difference that might be expected in going from Cr to Mn, the behavior of the bridging hydrogens in $HFe_4(CO)_{12}BH_2$ and $HFe_4(CO)_{12}CH$ was used as a guide. The pertinent data are given in Fig. 5 where it is seen that the hydrogen atom responds to a change from B to C by moving (ca. 0.5 Å) roughly parallel to the metal-main group atom vector towards the atom of higher electronegativity [24]. As the position of the Cr–H–B hydrogen of $Cp^*_2Cr_2B_4H_8$ lies close to the line established by the positions of the endo hydrogens of $HFe_4(CO)_{12}CH$ and $HFe_4(CO)_{12}CH$, the hydrogen atoms of $Cp_2Mn_2B_4H_8$ were moved ca. 0.2 Å along the line towards Mn. This modest change in geometry on the MO structure has a dramatic effect on two MO values (Fig. 3(b)). Because MO 43 is Mn–H antibonding (Fig. 4), moving the hydrogen atoms towards the Mn atoms destabilizes MO 43 and the HOMO–LUMO gap nearly doubles. MO 41 is modestly stabilized. Here the origin of the stabilization is less obvious but is mainly associated with a reduction in Mn–H antibonding character as the hydrogen atoms are moved relative to the Mn atoms. The overall result is a HOMO–LUMO gap similar to that of **1** and comparable Koopmans ionization energies (10.8 vs. 10.2 eV).

## 4. Conclusions

Although the stability of electronically unsaturated **1** is associated with significant Cr–Cr bonding originating from orbitals derived from the formally nonbonding '$t_{2g}$'set of the CpM fragment, the characterization of **3** shows further *decrease* in the M–M distance on the addition of two electrons to the cluster bonding network, e.g. in contrast $[CpCr(CO)_2]_2$ has a short Cr≡Cr triple bond whereas $[CpCr(CO)_3]_2$ has a long single bond. The change in cluster structure in going from **1** to **2** is consistent with the electronic structure change required to accommodate the additional pair of electrons.

An aspect of the problem that was hidden in the comparison of **1** with **3**, but revealed by **2**, is the important role of the endohydrogens in stabilizing the cluster structure for different electron counts. Sensitivity of cluster structure shape to the presence and placement of endohydrogens is known [25]. Indeed, it has also been reported that the calculation of $^{11}$B-NMR chemical shifts in boranes is sensitive to the placement of bridging hydrogens [26]. However, the sensitivity of a cluster with a fixed number of endohydrogens and cluster fragments to endohydrogen position has not

been unobserved previously. A consequence is that in **1** the hydrogens are clearly similar to those in boron hydrides whereas in **2** they are much more like metal hydrides. It is not surprising, then, that these differences are expressed in the different reactivities of the two compounds centered around the endohydrogens, e.g. **1** readily coordinates to a $Co(CO)_3$ fragment with the loss of a single endohydrogen [27] whereas all four endohydrogens are replaced in **2** by a $Co_2(CO)_5$ fragment [28].

## 5. Supplementary material

Crystallographic data for the structural analysis has been deposited with the Cambridge Crystallographic Data Centre, CCDC no. 141006 for compound **2**. Copies of this information may be obtained free of charge from The Director, CCDC, 12 Union Road, Cambridge, CB2 1EZ, UK (fax: +44-1223-336033; e-mail: deposit@ccdc.cam.ac.uk or www: http://www.ccdc.cam.ac.uk

## Acknowledgements

The support of the National Science Foundation is gratefully acknowledged. It is also appropriate to acknowledge the fact that Sheldon Shore introduced me to synthetic metallaborane chemistry in his laboratory during the summer of 1975. His hospitality, including flying excursions, are pleasant memories.

## References

[1] K. Wade, Adv. Inorg. Chem. Radiochem. 18 (1976) 1.
[2] D.M.P. Mingos, D.J. Wales, Introduction to Cluster Chemistry, Prentice Hall, New York, 1990.
[3] K.J. Deck, Y. Nishihara, M. Shang, T.P. Fehlner, J. Am. Chem. Soc. 116 (1994) 8408.
[4] J. Ho, K.J. Deck, Y. Nishihara, M. Shang, T.P. Fehlner, J. Am. Chem. Soc. 117 (1995) 10292.
[5] D.F. Shriver, H.D. Kaesz, in: R.D. Adams (Ed.), The Chemistry of Metal Cluster Complexes, VCH, New York, 1990.
[6] S.A.R. Knox, R.F.D. Stansfield, F.G.A. Stone, M.J. Winter, P. Woodward, J. Chem. Soc. Dalton Trans. (1982) 173.
[7] T.P. Fehlner, J. Organomet. Chem. 550 (1998) 21.
[8] S. Aldridge, T.P. Fehlner, M. Shang, J. Am. Chem. Soc. 119 (1997) 2339.
[9] T.P. Fehlner, J. Chem. Soc. Dalton Trans. (1998) 1525.
[10] K. Kawamura, T.P. Fehlner, Organometallics 17 (1998) 1904.
[11] D.F. Gaines, S.J. Hildebrandt, Inorg. Chem. 17 (1978) 794.
[12] D.E. Coons, D.F. Gaines, Inorg. Chem. 24 (1985) 3774.
[13] J.D. Kennedy, Prog. Inorg. Chem. 32 (1984) 519.
[14] J.D. Kennedy, Prog. Inorg. Chem. 34 (1986) 211.
[15] K.P. Gable, T.N. Phan, J. Organomet. Chem. 466 (1994) C5.
[16] W.A. Herrmann, E. Herdtweck, M. Floel, J. Kulpe, U. Kusthardt, J. Okuda, Polyhedron 6 (1987) 1165.
[17] G.M. Sheldrick, Siemens Industrial Automation Inc., Madison, WI, 1994.
[18] M.B. Hall, R.F. Fenske, Inorg. Chem. 11 (1972) 768.
[19] R.F. Fenske, Pure Appl. Chem. 27 (1988) 61.
[20] A.S. Weller, M. Shang, T.P. Fehlner, Organometallics 18 (1999) 853.
[21] H. Hashimoto, M. Shang, T.P. Fehlner, J. Am. Chem. Soc. 118 (1996) 8164.
[22] R. Poli, G. Wilkinson, M. Moetevailli, M.B. Hursthouse, J. Chem. Soc. Dalton Trans. (1985) 931.
[23] T.A. Albright, J.K. Burdett, H.H. Whangbo, Orbital Interactions in Chemistry, Wiley, New York, 1985.
[24] T.P. Fehlner, C.E. Housecroft, W.R. Scheidt, K.S. Wong, Organometallics 2 (1983) 825.
[25] W.W. Porterfield, M.E. Jones, K. Wade, Inorg. Chem. 29 (1990) 2923.
[26] M. Bühl, P.V. Schleyer, Angew Chem. Int. Ed. Engl. 29 (1990) 886.
[27] S. Aldridge, H. Hashimoto, K. Kawamura, M. Shang, T.P. Fehlner, Inorg. Chem. 37 (1998) 928.
[28] S. Ghosh, M. Shang, T.P. Fehlner, J. Am. Chem. Soc. 121 (1999) 7451.